CHEMICAL ENGINEERING TRANSACTIONS
VOL. 94, 2022
A publication of AIDIC
The Italian Association of Chemical Engineering
Online at www.cetjournal.it
Guest Editors: Petar S. Varbanov, Yee Van Fan, Jiří J. Klemeš, Sandro Nižetić

ISBN 978-88-95608-93-8; **ISSN** 2283-9216
DOI: 10.3303/CET2294093

Investigation and Modelling of Cylindrical Dividing Headers

Dominika Babička Fialová*, Zdeněk Jegla

Institute of Process Engineering, Faculty of Mechanical Engineering, Brno University of Technology, Technická 2, 616 69 Brno, Czech Republic
dominika.fialova@vutbr.cz

Flow maldistribution in tubular heat exchangers may cause severe thermal and mechanical operating problems. In this view, the crucial part of a distribution system is the inlet header. Nevertheless, a cylindrical header, the most common one in the process industry, distributes fluid flow into the tube bundle non-uniformly by its nature. One possible way to improve such unsuitable flow conditions is to gradually change the header height. However, variable header height is utilized mainly in equipment with a rectangular cross-section. So far, standard cylindrical headers have not been modified in such a way.
This study presents the results of an investigation into the flow behaviour in three dividing headers with circular cross-sections, two of which featured different changes to their height (linear decrease, optimised shape). The corresponding flow distributions were predicted via a simplified mathematical model as well as steady and transient CFD simulations. The obtained results were validated by experiments using additively manufactured headers, and it was found that the predicted flow distributions agreed with the observed trends. The conducted investigation also showed that the linear change of header height significantly improved flow distribution in the middle of the tube bundle. Nevertheless, the significant decrease in the tube flow rates near the distributor closed end caused degradation of the one-value maldistribution criterion compared to the value observed for the standard header design. The proposed modification of the header shape appears to be promising in terms of its future utilization in complete distribution systems and process heat exchangers, because it equalizes lateral flow rates in the middle of the tube bundle to the max. difference of ca. 2 % compared to ca. 6 % observed in the standard cylindrical shape.

1. Introduction

Flow distribution is one of the essential pieces of information to be determined when heat transfer equipment is being designed. The impact of flow distribution on reducing environmental footprints can be divided into two areas. Firstly, it can contribute to the mitigation of excessive thermal loading and extend the equipment lifespan (Fialová and Jegla, 2019). Secondly, uniform flow distribution not only increases the thermal effectiveness of the process equipment but also reduces its pressure drop, which results in lower investment and operating costs (Hajabdolahi and Seifoori, 2017). Efficient resource management makes it possible to considerably reduce external utility usage and lower emissions (Mahmood et al., 2021).
Flow maldistribution can be managed by various design modifications, e.g., by placing orifices into the tubes or baffles into the manifolds, or by varying the header cross-section. The latter approach has been applied mainly in equipment with cuboid manifolds, for example, an air preheater analysed by Turek et al. (2011) or mini channel systems investigated by Dąbrowski (2020). Ocłoń et al. (2021) successfully utilised linear changes in a header having semi-circular cross-section. So far, a linear change in header height has not been applied to standard cylindrical headers employed in the process industry. The influence of the suggested modification on flow distribution is examined together with the flow behaviour in a standard header.
Because the differential distribution model presented in a previous paper by Fialová and Jegla (2021) is only applicable to the standard, cylindrical geometry, a new method based on simple algebraic formulation had to be developed. Predictions obtained using the proposed algebraic model that is suitable also for systems with a non-negligible hydraulic resistance of lateral branches were compared with the results of detailed numerical simulations. These findings also were verified using data from physical experiments.

Paper Received: 14 April 2022; Revised: 13 May 2022; Accepted: 21 May 2022
Please cite this article as: Fialová D.B., Jegla Z., 2022, Investigation and Modelling of Cylindrical Dividing Headers, Chemical Engineering Transactions, 94, 559-564 DOI:10.3303/CET2294093

2. Modelling methods and examined designs of dividing headers

In this study, the effect of header shape on flow distribution was examined in three cylindrical headers. The default geometry (flow system I) constituted a standard cylindrical header with a constant circular cross-section, while the other two flow systems (II and III) featured different changes in header height. Each flow system included 14 lateral branches (tubes) with the inner diameter of 8 mm and the total length of 1.55 m. The branches were evenly spaced along the headers with the pitch being 50 mm. The relative header length (L/D ratio) is kept at 10; the initial value of cross-sectional area ratio A_r, i.e., the ratio of the tube cross-sectional area to the header inlet cross-sectional area, was approx. 1.

Figure 1 shows a schematic comparison of longitudinal sections of the three headers. Schematic of the respective header cross-sections (also displayed in Figure 1) show how a linear change of header height limits cross-sectional area to solely circular segments. A 30 mm long inlet zone was without any changes in height H (identical to the inner diameter D = 30 mm) in the case of all three headers. In the basic modification (flow system II), H then continuously decreased to 0 mm in case of a basic modification (flow system II). In flow system III with an optimized header shape, H decreased to 5 mm at the closed end of the header.

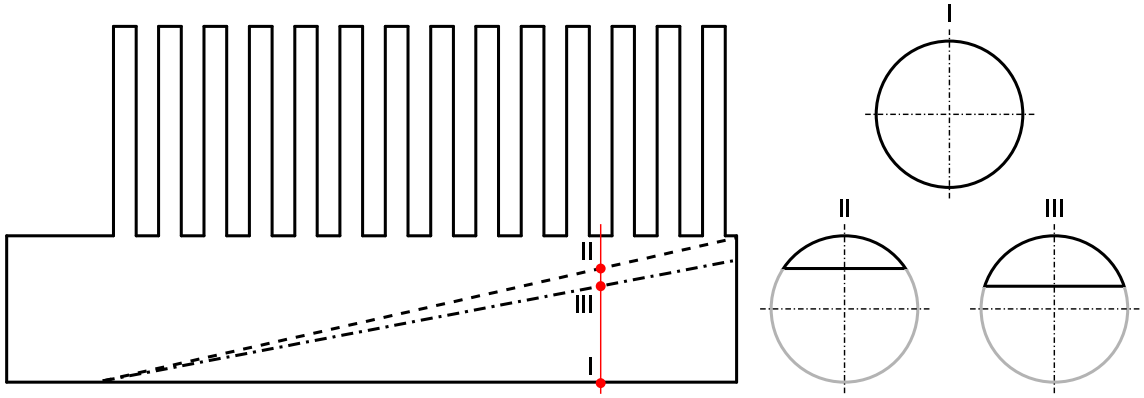

Figure 1: Schematic of the analysed headers – solid line denotes the cylindrical header (I), dashed line the basic linear modification of the header (II), and dash-dot line the optimized linear modification of the header (III)

2.1 Algebraic model

As the first approach to predicting flow distribution in the dividing header, a sufficiently accurate and computationally inexpensive method was sought. One of the crucial parameters of such a method was also its fast performance so that it could be employed in a header shape optimisation procedure (flow maldistribution being the objective function). The proposed simple algebraic model built upon Bailey's model (1975) and the modifications introduced by Turek et al. (2011) for manifolds with linearly changing rectangular cross-section.

The algebraic model dealt with pressure changes along the i-th section of the header using two fundamental equations (for nomenclature, please see Figure 2 showing a schematic comprising two branches and the header section between them). Eq(1) governed pressure regain caused by the changes in fluid momentum near the mouth of the i-th tube. This increase in pressure p_i between the flow just upstream (denoted by superscript "L") and just downstream (superscript "R") of the tube was computed using the coefficient $C_{r,i}$, i.e., the ratio of the difference in static pressures and the difference in dynamic pressures (represented by mean fluid velocities vi in the respective locations and fluid density ρ).

$$p_i^{\mathrm{R}} - p_i^{\mathrm{L}} = \frac{C_{\mathrm{r},i}}{2}\,\rho\left[\left(v_i^{\mathrm{L}}\right)^2 - \left(v_i^{\mathrm{R}}\right)^2\right] \tag{1}$$

Pressure loss due to the change in the header height and friction in the i-th header section was computed using Eq(2). Changes in header height (represented by cross-sectional areas A in three locations in the i-th section) and the respective pressure changes were included via the continuity and Bernoulli equations. Darcy–Weisbach equation (far right-hand term in Eq(2)) governed the pressure loss due to friction in the header. In Eq(2), fi denotes the Darcy friction factor for the i-th header section, D_h hydraulic diameter (the letter "M" denotes the middle of the section), and $L_{D,i}$ the length of this section.

$$p_{i+1}^{\mathrm{L}} - p_i^{\mathrm{R}} = \rho \frac{\left(v_i^{\mathrm{M}}\right)^2}{2} \left(A_{\mathrm{D},i}^{\mathrm{M}}\right)^2 \left(\frac{1}{A_{\mathrm{D},i}^2} - \frac{1}{A_{\mathrm{D},i+1}^2}\right) - f_i \frac{L_{\mathrm{D},i}}{D_{\mathrm{h},i}^{\mathrm{M}}} \rho \frac{\left(v_i^{\mathrm{M}}\right)^2}{2} \tag{2}$$

The presented model assumed steady incompressible flow. Further simplifications included constant fluid temperature and the effect of the gravitational field being neglected.
Volumetric flow rate $Q_{\mathrm{T},i}$ (i.e., discharge) through the *i*-th tube under the assumption of equal static pressures pout at all tube exits was calculated using the following equation:

$$Q_{\mathrm{T},i} = A_{\mathrm{T}} C_{\mathrm{d},i} \left[\frac{2}{\rho}\left(\frac{p_i^{\mathrm{R}} + p_i^{\mathrm{L}}}{2} - \Delta p_{\mathrm{T},i} - p_{\mathrm{out}}\right)\right]^{0.5} \tag{3}$$

In Eq(3), $C_{\mathrm{d},i}$ denotes the discharge coefficient for the *i*-th tube as defined by Bailey (1975), $A_{\mathrm{T},i}$ the cross sectional area of the tube, and $\Delta p_{\mathrm{T},i}$ the overall tube pressure drop (pressure loss caused by friction as well as possible minor losses in the tube).

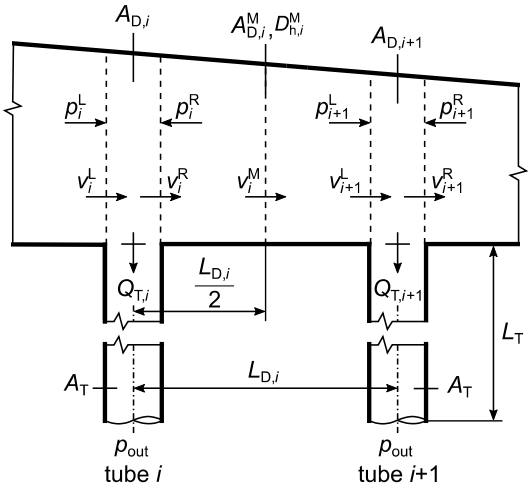

Figure 2: Schematic of the i*-th header section having a linearly varying height*

2.2 CFD modelling

Predictions of the flow behaviour, obtained using the algebraic model, were compared with the results of detailed Computational Fluid Dynamics (CFD) simulations carried out in Ansys Fluent (Ansys Inc., 2021). The isothermal condition was maintained in all simulations of water flow through the headers. The respective CFD cases were set up as follows:

- Pressure-based solver with absolute velocity formulation and double-precision;
- Enhanced wall treatment with realizable *k*–*ε* model;
- SIMPLE algorithm for pressure–velocity coupling and Green–Gauss node based gradient calculation;
- Spatial discretization: second order for pressure, second order upwind for density, momentum, turbulent kinetic energy, and turbulent dissipation rate;
- Boundary conditions: mass flow inlet (0.7056 kg/s), pressure outlet (gauge pressure 0 Pa), porous jump in the tubes (pressure-jump coefficient of 4.85 m^{-1} and porous medium thickness of 1.35 m), no-slip wall.

As for the transient cases, the time steps were adjusted according to the Courant number for the respective geometry. Transient simulations were terminated after the flow rates had stabilized for at least 40 s.
A significant shortening of the modelled tubes via the porous jump boundary condition (from 1.55 m to 0.20 m) and the variable mesh density enabled a considerable cell count savings. Consequently, it was possible to avoid overly high computational costs. Usage of the variable mesh density also ensured that appropriate values of mesh quality criteria (e.g., maximum skewness under 0.79) were met in the most critical regions where large gradients of flow variables could be expected.
In order to identify optimum grid resolution, a grid independence study described in detail by Fialová and Jegla (2021) was performed using the constant cross-section geometry. The most suitable mesh consisted of 3.85 M polyhedral cells. Both modified header geometries also adopted the respective fine-tuned mesh setting with

additional refinements being done at the closed ends of the headers. The resulting mesh sizes were 4.12 M and 3.82 M in the case of the basic modification and the optimized shape.

2.3 Experimental setup

The experimental headers with short, 50 mm tubes were manufactured additively via Fused Deposition Modelling (FDM) from Acrylonitrile Butadiene Styrene (ABS) using the Trilab DeltiQ XXL 3D printer by TriLAB Group s.r.o. (Brno, Czech Republic). The samples were printed in the vertical position using the 0.12 mm thick layer and 100 % infill. After removing the supporting structures from the tubes, post-processing tasks proceeded with machining inner diameters of the tubes and the outer surfaces of the headers were treated with acetone.
The printed tubes were extended by plain, 1.8 m long polyurethane (PU) hoses. The test facility was kept as simple as possible to avoid minor losses caused by measuring instruments (e.g., variable area flowmeters or orifices). The inlet flow rate was controlled using a ball valve and measured via an electromagnetic flowmeter SM 8000 (IFM Electronic). Inlet pressure was measured using a pressure sensor PN 2594 (IFM Electronic). Water temperature, needed to calculate its physical properties, was measured using a PTS 360 sensor (Sensit). The tube flow rates were measured via the cumulative method (Fialová and Jegla, 2021). Each experiment was repeated three times. Please see (Fialová and Jegla, 2021) for detailed information regarding the experimental setup.

3. Results and discussion

The algebraic model was implemented into a simple optimisation procedure in Maplesoft Maple (Maplesoft, 2019) which assumed linear changes of the header height. Height at the closed end of the header was selected by the code such that the lowest flow maldistribution was reached. Flow distribution non-uniformity was evaluated via the relative standard deviation (RSD) from uniform flow distribution. The best value of RSD was obtained using the geometry which featured the closed end height of 5 mm.
Lateral flow rates and the overall pressure drop yielded by the algebraic model and CFD simulations were compared with experimental data. Please note that flow rates corresponding to transient CFD simulations were arithmetic means corresponding to large numbers of values obtained using 40 s of computational time. For the sake of simplicity, each lateral flow rate was normalised using the average flow rate from the corresponding physical experiment. These scaled values are shown in Figures 3–5.
It is obvious from Figures 3–5 that there is a good agreement between the flow rates reported by the CFD simulations and those obtained via physical experiments. It is also apparent that the steady simulations yielded flow distributions similar to those from the transient (costlier) models. However, the default scaled residual limits had to be decreased in Ansys Fluent to 10^{-4} for the flow variables to stabilise (for a detailed description, please see the previous work by Fialová and Jegla, 2021). The best agreement between experimental data and predictions of the algebraic model was reached with flow system II. Especially in the case of flow system III, the algebraic model was not able to predict the extremely low flow rates in the peripheral tubes. The maximum relative differences between the measured and predicted tube flow rates and their locations in the test flow systems are listed in Table 1. It also should be noted that the simplified mathematical model presented in (Fialová and Jegla, 2021) can predict better the trend for flow distribution in the basic flow system I than the algebraic model discussed here.
Considering the RSD criterion and pressure drops (also mentioned in Table 1), the data indicate relatively good agreement between CFD simulations and experiments. The algebraic model overestimates the pressure drops, which also affects the final value of RSD.

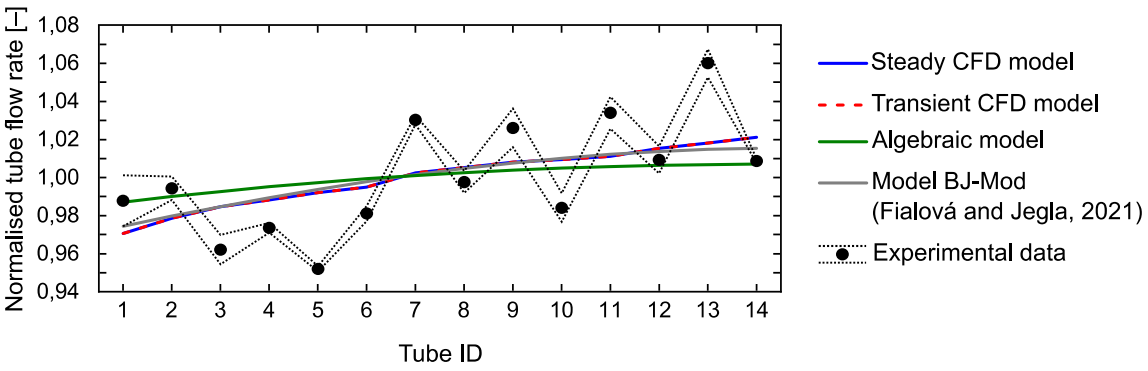

Figure 3: Normalised tube flow rates obtained using flow system I

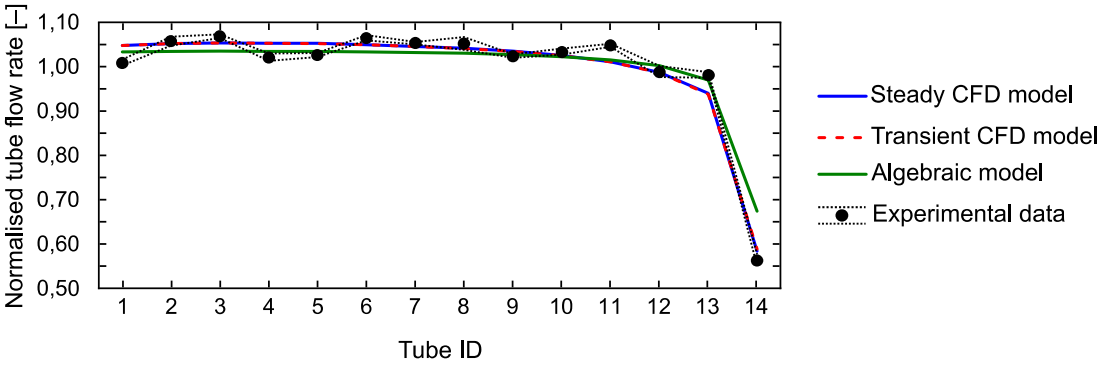

Figure 4: Normalised tube flow rates obtained using flow system II

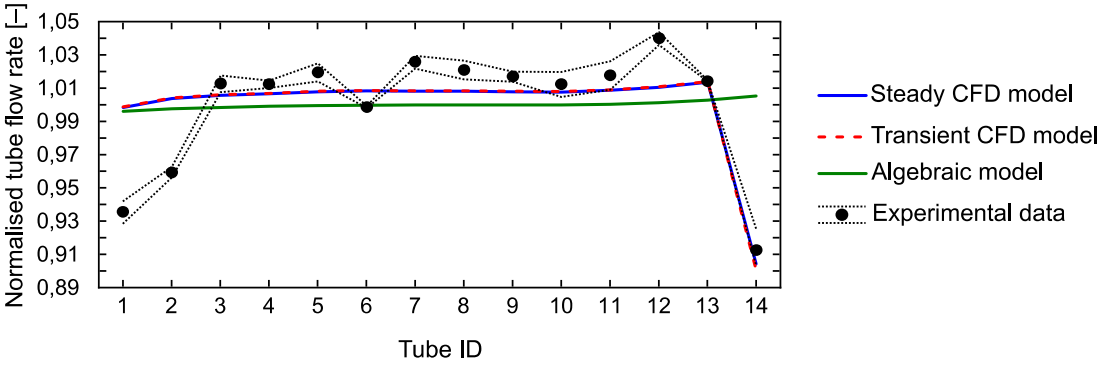

Figure 5: Normalised tube flow rates obtained using flow system III

Table 1: Flow maldistributions and pressure drops related to the testing flow systems

	Algebraic model	Steady CFD model	Transient CFD model	Experimental data
Flow system I				
RSD, %	0.64	1.49	1.49	2.90
Max. rel. difference of flow rate, %	4.77 (5th tube)	4.23 (5th tube)	4.23 (5th tube)	–
Pressure drop, Pa	5,058	5,200	5,464	5,017
Flow system II				
RSD, %	8.45	11.96	11.85	12.39
Max. rel. difference of flow rate, %	19.72 (14th tube)	3.93 (1st tube)	4.50 (14th tube)	–
Pressure drop, Pa	6,040	5,965	5,963	5,925
Flow system III				
RSD, %	0.21	2.67	2.77	3.57
Max. rel. difference of flow rate, %	15.49 (14th tube)	6.73 (1st tube)	6.76 (1st tube)	–
Pressure drop, Pa	5,258	5,463	5,465	5,492

As for the effect of header shape on flow maldistribution, the value of the RSD criterion in the optimised flow system III was slightly larger (i.e., worse) than the RSD in the standard geometry (flow system I). However, the linear change of header height improved flow distribution in the central part of both flow systems II and III. The proposed shape modifications can equalize flow rates in tubes 3–12 (the maximum difference being ca. 2 % compared to ca. 6 % for the same tubes in flow system I).

4. Conclusions and future work

A linear change in a cylindrical distributor header height has been proposed. The investigation of flow distribution in several modified headers has revealed promising results. In the middle of the tube bundle, the optimised shape has been able to stabilise normalised flow rates at 101 % ± 1 %. In comparison, the standard cylindrical header has yielded normalised flow rates of 100 % ± 3 %. Still, further adjustments of the header shape, e.g.,

axial shift of the point where the cross-section starts to change, must be examined. These additional adjustments may significantly influence the extreme flow rates observed in the peripheral tubes.
It has been shown that the proposed algebraic model can yield reasonably accurate predictions of flow trends in dividing headers with linear changes of their height, although its accuracy in the case of the standard cylindrical headers is lower compared to the original differential model. To overcome this major downside, the empirical equations utilized to calculate the two key coefficients (C_r, C_d) must be investigated further. The obtained experimental data have also revealed that transient CFD simulations do not significantly improve accuracy compared to the less computationally demanding steady ones.
Finally, the performance of the proposed header modifications must be analysed in the context of a complete distribution system (incl. the collection header). Such experiments are planned for the near future.

Acknowledgments

The presented research was supported by GA BUT within the research project FSI-S-17-4526. The authors appreciate the assistance in additive manufacturing provided by the REAT Department IMID, FME BUT. The authors are grateful to the employees of the Laboratory of Energy Intensive Processes (NETME Centre and IPE, FME BUT) for their support during experiments.

Nomenclature

Symbols:

A –cross-sectional area, m^2
A_r – cross-sectional area ratio, -
C_d – discharge coefficient, -
C_r – coefficient of static pressure regain, -
D – inner diameter of header, m
D_h – hydraulic diameter, m
f – Darcy friction factor, -
H – header height, -
k – turbulence kinetic energy, $m^2\ s^{-2}$
L – length, m
L/D – relative header length, -
n – number of tubes, -
p – static pressure in header, Pa
p_{out} – pressure at tube outlet, Pa
Q – volumetric flow rate, $m^3 \cdot s^{-1}$
RSD – relative standard deviation, %
v – mean fluid velocity in header, $m \cdot s^{-1}$
Δp – pressure drop, Pa
ε – rate of dissipation of turb. kin. energy, $m^2\ s^{-3}$
ρ – fluid density, $kg \cdot m^{-3}$

Superscripts and subscripts:

D – header
i – index of tube or header section
L – quantity just upstream of a tube
M – quantity in the middle of a section
R – quantity just downstream of a tube
T – tube

References

ANSYS Inc., 2021, ANSYS Fluent User's Guide, Version 2021 R1. ANSYS, Inc., Canonsburgh, USA.
Bailey B.J., 1975, Fluid flow in perforated pipes, J. Mech. Eng. Sci., 17, 338–347, DOI:10.1243/JMES_JOUR_1975_017_048_02.
Dabrowski P., 2020, Thermohydraulic maldistribution reduction in mini heat exchangers, Appl. Therm. Eng., 173, 115271, DOI:10.1016/j.applthermaleng.2020.115271.
Fialová D., Jegla Z., 2019, Analysis of fired equipment within the framework of low-cost modelling systems, Energies, 12, 520, DOI:10.3390/en12030520.
Fialová D.B., Jegla Z., 2021, Experimentally verified flow distribution model for a Composite Modelling System, Energies, 14,1778, DOI:10.3390/en14061778.
Hajabdollahi H., Seifoori S., 2016, Effect of flow maldistribution on the optimal design of a cross flow heat exchanger, Int. J. Therm. Sci., 109, 242-252, DOI: 10.1016/j.ijthermalsci.2016.06.014.
Mahmood Z., De Mel I., Kazi S.R., Isafiade A.J., Short M., 2021, An optimisation algorithm for detailed shell-and-tube heat exchanger designs for multi-period operation, Chem. Eng. Trans., 88, 253–258, DOI:10.3303/CET2188042.
MAPLESOFT, 2019, Maple User Manual. Waterloo Maple, Inc., Waterloo, ON, Canada.
Ocłoń P., Łopata S., Stelmach T., Li M., Zhang J.F., Mzad H., Tao W.Q., 2021, Design optimization of a high-temperature fin-and-tube heat exchanger manifold—A case study, Energy, 215, 119059, DOI:10.1016/j.energy.2020.119059.
Turek V., Hájek J., Jegla Z., Stehlík P., 2011, Optimum design of fluid distribution systems in heat exchangers, Asia-Pac. J. Chem. Eng., 6, 750–759, DOI:10.1002/apj.516.